Protection of converter dominated MV microgrid using changes in current's phase angle

Received: 4 March 2021 | Revised: 8 September 2021 | Accepted: 22 September 2021

IET Generation, Transmission & Distribution

DOI: 10.1049/gtd2.12317

The Institution of Engineering and Technology WILEY

ORIGINAL RESEARCH PAPER

Protection of converter dominated MV microgrid using changes in current's phase angle

Rabindra Mohanty[1,2] | **Peiyuan Chen**[1] | **Le Anh Tuan**[1]

[1] Division of Electric Power Engineering, Department of Electrical Engineering, Chalmers University of Technology, Gothenburg 41296, Sweden

[2] Department of Electrical & Electronics Engineering, BITS Pilani, Hyderabad, Telangana 500078, India

Correspondence
Rabindra Mohanty, Division of Electric Power Engineering, Department of Electrical Engineering, Chalmers University of Technology, 41296 Gothenburg, Sweden; Department of Electrical, and Electronics Engineering, BITS Pilani, Hyderabad, Telangana 500078, India.
Email: rabindramohanty.ee@gmail.com

Funding information
Energy Area of Advance at Chalmers University, Grant/Award Number: WP A6; Sweden Energy Agency under SamspEL program, Grant/Award Number: P43014-1; FLEXI-GRID, European Community's Horizon 2020 Framework Programme, Grant/Award Number: 864048

Abstract

Converter interfaced distributed generations in a microgrid feed the modulated current of limited magnitude during fault conditions. The protection design and its operation are thus challenging due to limited fault current which is further reduced by Petersen coil grounding in medium-voltage (MV) level. This paper aims to address this challenge by developing a current-only directional relay algorithm for the protection of converter dominated MV microgrid with Petersen coil grounding. The relay's operating principle is based on the sign of the change in phase angle of the fault current with respect to the prefault which indicates the direction of fault. The negative and positive changes in current's phase angle determine the fault in forward and reverse direction, respectively. The tripping decision is derived by comparing the binary output of the relay at both ends of the line segment under protection. This requires a simple, flexible and low bandwidth communication channel. Both theoretical analyses and simulation studies have been performed on a typical distribution grid intended to be operated as microgrid. The proposed protection method is suitable for microgrid having the converters with and without reactive power support. Various operating conditions are evaluated, including bidirectional power flow, high resistance fault, different fault types, loading conditions and signals with noise.

1 | INTRODUCTION

Microgrid is now a reliable energy solution of electrifying remote areas and smart cities at low- or medium-voltage level [1]. Renewable-powered generators, such as solar photovoltaic (PV), wind turbines and battery energy storage systems (BESSs) are usually connected to the microgrid through voltage source converters (VSCs) [1, 2]. The current contribution from VSC during fault condition is dominated by its control and limited to rated current. Such a low fault current makes it difficult for the traditional overcurrent relay to detect the fault [3]. If the fault is not detected and cleared in due time, there may be significant damage to the equipment exposed to the fault current. In practice, one way to solve this problem is to overdimension the converter of the BESS so that it can provide, for example, three times the rated load current under fault conditions and make it suitable for conventional overcurrent relay operation. This, however, requires additional investment cost on the converter, and also reduces the converter efficiency during normal operation.

Furthermore, overhead lines in distribution grids are commonly replaced by underground cable to improve power supply reliability by reducing interruption due to poor weather conditions [4]. In underground cable systems, faults are more likely to be permanent and the charging current is significant, especially for a phase-to-ground fault. The total charging current at fault point is three times that of per phase in normal operation [5]. Petersen coil is used for the neutral grounding of MV distribution transformer to compensate the charging current during the ground faults [6].

Converters are typically ungrounded and generate only positive-sequence current even during unbalance fault [7, 8]. Negative- and zero-sequence-based directional relays are not reliable for the protection of converter dominated microgrids

[9]. Current differential principle is still a suitable protection method of such a microgrid due to its invulnerable nature to bidirectional power flow, fault current levels, distributed generation (DG) location and operating modes [10, 11]. This would require the installation of differential protection at each section of a feeder, with high bandwidth communication and low time synchronization error. These make it an expensive investment [12]. Furthermore, the differential protection may fail to operate under high resistance fault. In addition, the non-identical nature of current at both ends of the cable segment due to the influence of different converter control makes it difficult to set the parameter of the differential protection properly [13, 14].

To tackle the fault detection and protection issues with limited fault current, authors in [15] propose traveling-wave-based protection for converter dominated microgrids. The initial current-wavefront feature is used for the fault detection. However, in practice, the distance between the buses are not long in microgrids and hence, the initial current-wavefront will not be accurate for selective operation of protective devices. In [16], a protection method for microgrid is proposed using positive sequence components of voltage and current. The protection issue with bidirectional power flow is not studied in [16], despite the method uses additional voltage measurement for protection decision. A multi-agent-based directional overcurrent protection scheme for traditional distribution systems is proposed in [17]. However, this method does not address the issues related to microgrid protection. The protection selectivity issue is handled in [18] using *abc-dq* transformation of voltage-based method in microgrids. For a fault, the q-component of voltage exceeds the predefined set value and trip signal is generated for the corresponding circuit breaker to achieve the selectivity. However, the voltage-based protection is not sensitive in case of the fault with high resistance and at the remote-end of a long feeder. Another important issue associated with protection selectivity is bidirectional power flow in microgrids. Current-based protection without directional property cannot identify the fault in forward or reverse direction, and thus directional relay is a solution for selective protection of microgrids. However, the conventional overcurrent directional relay uses voltage information as a reference quantity and the phase angle difference of current with respect to the voltage reference estimates the direction of fault [19]. This would require additional investment on voltage transformer in distribution systems [20]. Moreover, the operation of conventional directional relay is unreliable for a close-in-fault that causes voltage collapse at relay point resulting unavailability of reference voltage quantity. Therefore, current-only directional relay will be a more reliable and economic solution for microgrids.

Typically, the communication-assisted protection schemes are more effective for converter dominated microgrids [11, 21]. Such methods will be more viable and adoptable, if the cost of communication will be reduced by any means. One way to make the low-cost communication system is by exchanging minimum information using low bandwidth channel between relays [14]. However, high resistance fault and its effects on fault current direction during different loading conditions are not considered in [14]. In [22], communication-assisted protection using artificial neural network (ANN)-based overcurrent protection is proposed to determine the direction of fault in microgrids. Adapting the ANN, centralized controller and zone controller are used for coordination of the protection devices and correct faulted segment identification. Nonetheless, the method requires time synchronized data and only applicable to grid connected microgrids. A mixed integer linear-program-model-based protection coordination method in distribution network is proposed in [23], where the technique is suitable for radial systems without consideration of DG integration. Similarly, another method in [24] for protection coordination of microgrid requires additional voltage measurement to obtain q-component of current.

This paper proposes an algorithm that uses the angle change of the positive-sequence current to derive the protection decision. The positive and negative change in phase angle turn to the binary status as 1 and 0, respectively. The trip signal is enabled based on XOR gate logic output, for example, unequal binary status at both ends of the line segment. Evaluation of the proposed algorithm is performed using simulation study on a yet typical network for various cases including no load, loading conditions, high resistance fault and bidirectional power. The main contributions of the paper include the following:

- Development of a new protection algorithm based on current-only directional principle to address the limited fault current due to converter's current limiting capability.
- The proposed algorithm does not use voltage measurement and only transfers binary signal during a disturbance. Therefore, low cost communication channel with low bandwidth is required.
- For a fault in a microgrid, the current fed by the VSC depends on the control strategy adopted. Detailed analysis of fault current contribution by VSC with and without reactive power support is carried out.
- Fault current limitation due to Petersen coil grounding for a ground fault is also addressed.
- The proposed algorithm is able to detect all types of shunt faults.
- The algorithm performs well for high resistance fault, even when the direction of current at remote end does not alter.

The rest of the paper is organized as follows. Section 2 describes protection issues including a Petersen coil grounding network. The current contributed by the VSC along with the theoretical analysis is presented in Section 3. The proposed current's phase-angle-change-based protection algorithm is presented in Section 4. In Section 5, the simulation results of the proposed algorithm are shown. Finally, the conclusion of the work is provided in Section 6.

2 | PROTECTION OF MEDIUM-VOLTAGE MICROGRID WITH PETERSEN COIL GROUNDING

A medium-voltage microgrid of 10 kV is shown in Figure 1. The microgrid operates as grid-connected and islanded modes

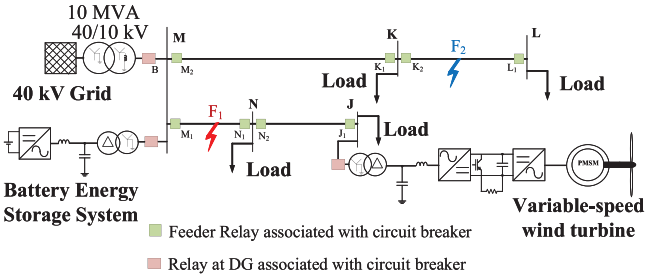

FIGURE 1 A medium-voltage microgrid with converter interfaced sources

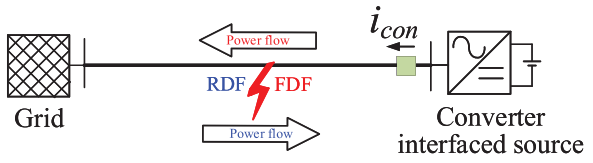

FIGURE 2 Fault current from a converter during forward and reverse direction fault

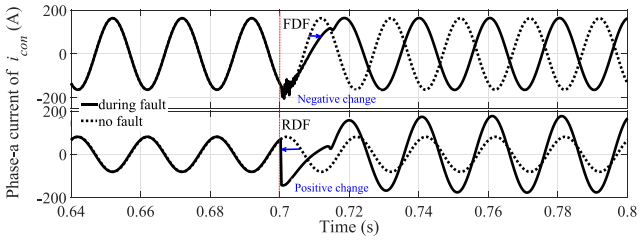

FIGURE 3 Change in converter current pattern for forward fault (above) and reverse fault (below)

with closing and opening of breaker B, respectively. Wind turbine with converter is integrated to the microgrid at bus J. BESS interfaced with VSC is connected at the substation bus M to keep the power balance of the microgrid operation. The neutral of star connected winding of the utility grid substation transformer is grounded through Petersen coil (PC) to have the advantages of both grounded and ungrounded systems. Furthermore, the neutral of star connected transformer at wind turbine and BESS is solidly grounded to allow the zero-sequence current flow during a ground fault in the microgrid.

In local grids, underground cables are used for power transfer with improved supply reliability by reducing the interruption due to bad weather conditions [4]. The charging current in such a cable dominated system causes serious concern during ground faults. Therefore, in Europe, it is suggested to ground the neutral of star connection of the substation transformer through a PC to minimize the capacitive earth current during earth faults [25]. For a line-to-ground fault, the zero-sequence current is canceled by the PC and the total fault current magnitude is determined by the grounding resistor connected in parallel to PC. Thus, conventional phase overcurrent and earth-fault protections do not operate for such a low current with no zero-sequence in PC grounding systems. The neutral voltage (V_n) displacement and initial transient behavior of zero-sequence current are used for ground fault detection, and the parallel resistor helps in identification of the correct faulted feeder [25]. However, V_n is not decisive for a ground fault with high resistance (small displacement of V_n) and network unbalance during non-fault (large displacement of V_n) situations. These issues related to phase overcurrent relays and V_n displacement are associated with grid-connected converter dominated microgrid with substation transformer grounded through PC. In islanded mode, the effect of PC disappears for ground faults and hence, the zero-sequence current flows. Note that the flow of zero-sequence current highly depends on the transformer connection of DG. In this case, the earth-fault protection operates correctly and can be considered as a backup protection [26, 27]. However, in case of ungrounded neutral of the transformer at DG, there will be no zero-sequence current flowing in the islanded microgrid during a ground fault. In this case, the available overcurrent and earth-fault protections cannot provide a reliable solution for converter dominated microgrids. The protection issues and challenges of converter dominated MV microgrids are further described in [28]. The proposed method addresses such issues and provides a protection solution based on the sign of change of current's phase angle.

3 | NATURE OF CURRENT FROM CONVERTERS

A fault leads to a change in not only voltage magnitude but also in phase angle [29, 30]. This also leads to the change in current angle before and during the fault. The increasing or decreasing of current angle depends on the fault impedance, types, location and prefault power flow direction. Figure 2 shows a simplified system with a converter interfaced source that is capable of delivering and absorbing both active and reactive current for explaining the basic of angle change. This paper focuses on converter current and therefore, the nature of i_{con} is analyzed for the forward direction fault (FDF) and reverse direction fault (RDF). In this case, only phase-a current of i_{con} is plotted as shown in Figure 3. It is observed that, the phase angle of i_{con} is changing negative and positive direction during FDF and RDF, respectively.

The above approach is further extended to three phase systems of current contribution from converter with controller. The VSC connecting the wind turbine to the microgrid acts as a grid following source and the inverter interfaced BESS acts as grid supporting source [31]. The phase angle of current depends on the amount of active (I_d) and reactive (I_q) components of current provided by the converter during fault [32]. The charging current is reactive in nature that could be added or subtracted to the reactive (q-component) current provided by the VSC in the faulted phase. Furthermore, the reactive current is defined by the grid code followed by the system operator. In this paper, E.ON grid code is considered as shown in Figure 4 [33, 34]. The VSC controls the active component of current at 1 p.u. with no reactive component for voltage more than or equal to 0.9 p.u. For the voltage dip of less than 0.9 p.u., the VSC starts

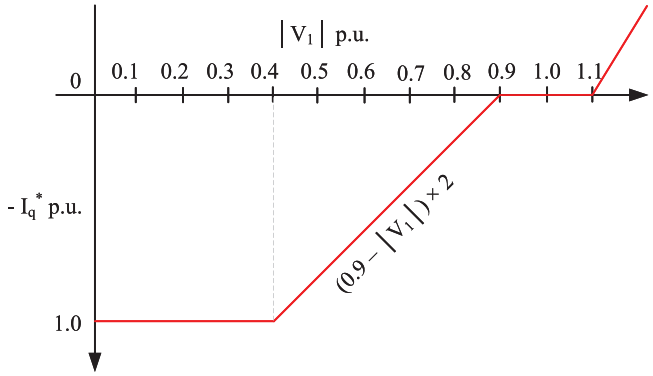

FIGURE 4 Reactive power support with respect to voltage at PCC

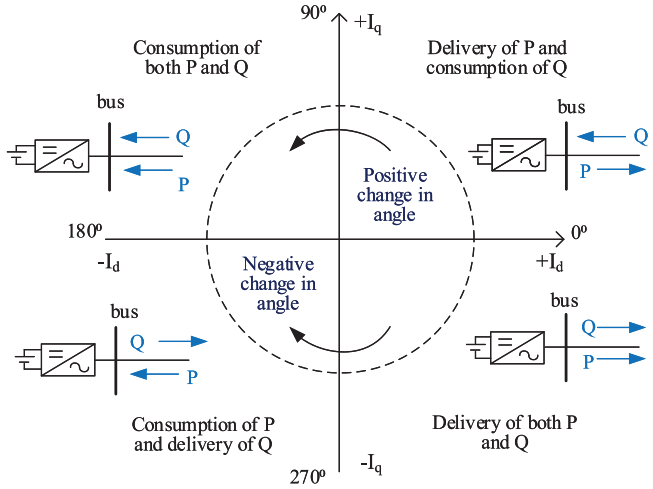

FIGURE 5 Sign convention of d- and q-component of current entering to and leaving from a bus during fault

injecting reactive current with a reference, twice of (0.9 - $|V_1|$). In case of voltage below 0.4 p.u., the VSC provides only reactive current of its full capacity. Figure 5 shows a four quadrant plane of I_d and I_q with the sign convention of power flow assumed in this paper. From (1), converter delivers both P and Q with positive I_d and negative I_q, thus the case is shown in fourth quadrant in Figure 5. Similarly, P-jQ, −P + jQ and −P − jQ will be in first, third and second quadrants, respectively.

$$P + jQ = V_d I_d - jV_d I_q. \quad (1)$$

Different factors are considered when evaluating current angles, including prefault power flow direction, load power factors, fault resistance, and reactive current support from VSC. Table 1 summarizes these different possible cases which are broadly categorized into four different study cases as below:

3.1 | Case 1—Fault current contribution from both ends

Figure 6 shows a low resistance fault at the middle of the line segment MN and all other sources are represented by their Thevenin equivalent of Figure 1. The currents from M and N sides to the fault point have both active and reactive components (being no/light load at bus N). In this case, the fault currents fed from both ends are inductive which is evident from the phasor diagrams of Figure 7. The change in phase angles during fault with respect to prefault are negative and positive at M and N sides, respectively. In the Swedish medium voltage network, the free annual reactive power exchange with the Vattenfall utility grid is 25% [35]. This corresponds to 0.95 lagging/leading pf with currant's phase angle varying between ± 18° (Figure 7). Even with such a value of initial phase angle of current, the proposed angle-change-based method performs correctly.

3.2 | Case 2—High resistance fault during full load unity pf

Figure 6 shows the direction of currents for a high resistance fault during full load condition with unity pf at bus N. This causes the division of total active component of current fed from M into fault loop and load. From the phasor diagram shown in Figure 8, it is clear that I_{MN} shifted to fourth-quadrant and I_{NM} to third-quadrant. Hence, the change in angle of current at M and N sides are negative and positive, respectively.

3.3 | Case 3—High resistance fault during full load lagging pf

This case is studied about the lagging pf loading. During full load condition, if a high resistance fault occurs, the direction of active and reactive component of current are shown as in Figure 6. The fault current at M and N are in fourth- and second-quadrant, respectively (refer Figure 9). This leads to a negative change in phase angle of the currents at both ends. Therefore, another feature is added to take the correct protection decision based on magnitude change in positive-sequence current. For a high resistance fault, the direction of current in the remote end of the faulted segment does not alter (Figure 9). In addition, the active and reactive components of current reduce in magnitude as the shunt fault comes in parallel to the load. Thus, $|I_{NM}^{F_1}| < |I_{NM}|$, or $\Delta I_{NM} = |I_{NM}^{F_1}| - |I_{NM}|$ is negative. Note that the sign of $|\Delta I_{NM}|$ during the high resistance fault depends on the type of loading at bus N. Such as

$$\Delta I_{NM} = \begin{cases} \text{negative}, & \text{if constant impedance load} \\ \text{positive}, & \text{constant power load} \\ \text{zero}, & \text{constant current load} \end{cases}$$

In this paper, constant impedance load is considered. The settings of the proposed protection can be modified according to prior knowledge on type of loading in the systems.

3.4 | Case 4—Fault on a radial and unidirectional power flow feeder

In this case, in Figure 6, a fault is occurred in the line segment MN with no power (P and Q) output from the DG at bus J. The

TABLE 1 Various operating conditions during a fault in the microgrids as shown in Figure 1

Reactive current support	Operating condition: Prefault power flow is from M to N		Fault in the line segment MN							
			Bolted fault				Fault with high R_f			
			I_{MN}		I_{NM}		I_{MN}		I_{NM}	
			I_{dM}	I_{qM}	I_{dN}	I_{qN}	I_{dM}	I_{qM}	I_{dN}	I_{qN}
DG without reactive current support	Feeding from both M and N	Heavy loading (case 2)	I_{dM}	0	$I_{dN}<$	0	I_{dM}	0	$I_{dN}<$	0
		No/light loading (case 1)	I_{dM}	0	$-I_{dN}$	0	I_{dM}	0	$-I_{dN}$	0
	Feeding from M side	Heavy loading (case 3)	I_{dM}	0	$I_{dN}<$	0	I_{dM}	0	I_{dN}	0
		No/light loading (case 4)	I_{dM}	0	0	0	I_{dM}	0	0	0
DG with reactive current support	Feeding from both M and N	Heavy loading (case 2)	I_{dM}	I_{qM}	$-I_{dN}$	$-I_{qN}$	I_{dM}	I_{qM}	I_{dN}	I_{qN}
		No/light loading (case 1)	I_{dM}	I_{qM}	$-I_{dN}$	$-I_{qN}$	I_{dM}	I_{qM}	$-I_{dN}$	$-I_{qN}$
	Feeding from M side	Heavy loading (case 3)	I_{dM}	I_{qM}	$I_{dN}<$	$I_{qN}<$	I_{dM}	I_{qM}	I_{dN}	I_{qN}
		No/light loading (case 4)	I_{dM}	I_{qM}	0	0	I_{dM}	I_{qM}	0	0

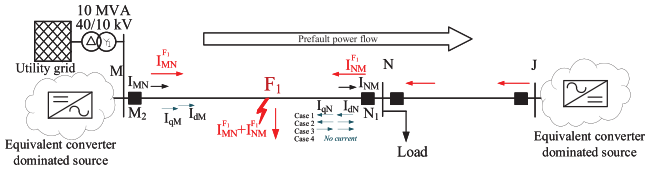

FIGURE 6 Faulted segment MN of the system shown in Figure 1

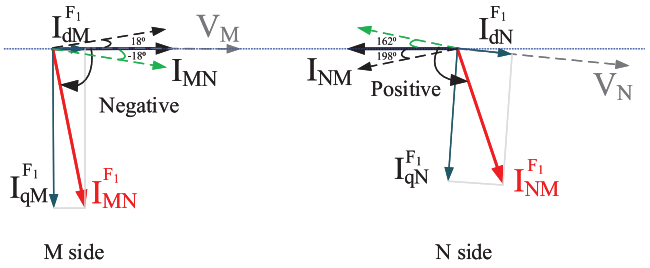

FIGURE 7 Case 1 - Phasor diagram during low resistance fault on the line segment MN

fault current is fed from M side only. The phasor diagram in Figure 10 shows that the change in phase angle of I_{MN} is negative. For a fault during no load conditions, there is no current available at N. Moreover, for a high resistance fault during full load, the fault current at N side will be in second-quadrant, and hence,

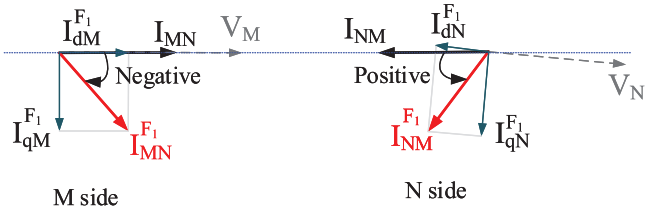

FIGURE 8 Case 2 - Phasor diagram diagram during high resistance fault and heavy loading conditions

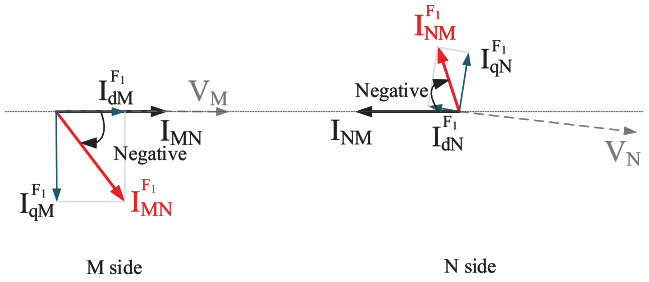

FIGURE 9 Case 3 - Phasor diagram during a high resistance fault and no reactive current support from N side

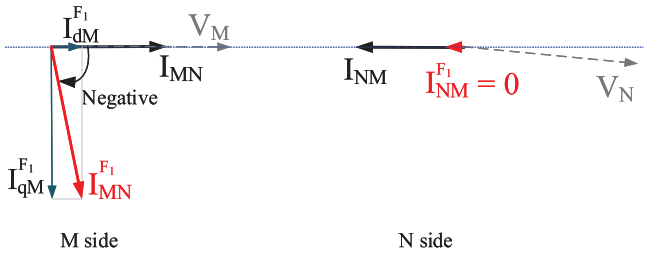

FIGURE 10 Case 4 - Phasor diagram during a low resistance fault with no load in single source radial network

negative angle change. The protection decision will be taken based on the criterion of superimposed positive-sequence current ΔI_{NM1}. In this case, the value is negative as described above.

4 | PROPOSED PROTECTION ALGORITHM

In this paper, the positive-sequence current is used to develop the proposed protection algorithm. By this, the limitation persists with the absence of negative-sequence component in converter output is overcome. Further, positive-sequence current is

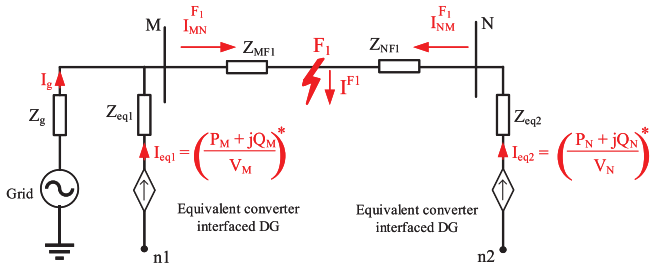

FIGURE 11 Equivalent positive-sequence circuit diagram during a three phase fault

present in all types of faults. An ideal protection scheme deals with two important steps, that is, fault detection followed by the protection decision.

4.1 | Fault detection

Unlike conventional distribution systems, the sample-to-sample or cycle-to-cycle approach cannot be used for fault detection in converter dominated microgrid as the current is limited to 1 p.u. within a cycle during fault [36]. Fault detection using sequence components of current could be an alternative in microgrids [32]. However, converter with negative-sequence control and balanced fault do not contain negative- or zero-sequence components. Therefore, a fault detection method is proposed using d- and q-components of current as follows:

$$\frac{\left|\Delta \mathrm{I_{qM}}\right|}{\left|\Delta \mathrm{I_{dM}}\right|} \geq 0.02, \tag{2}$$

where $\Delta \mathrm{I_{qM}} = \mathrm{I_{qM}}(\mathrm{t_2}) - \mathrm{I_{qM}}(\mathrm{t_1})$ and $\Delta \mathrm{I_{dM}} = \mathrm{I_{dM}}(\mathrm{t_2}) - \mathrm{I_{dM}}(\mathrm{t_1})$ are the change in q- and d-components of current at bus M. The threshold is set as 0.02 as the followed grid code suggests 2% increase in I_q for the voltage drop of every 1% below 0.9 p.u. A fault or disturbance is confirmed if three consecutive ratio exceeds the threshold.

In the Figure 11, the positive-sequence equivalent circuit diagram is shown during the fault F_1. The total fault current can be expressed as

$$\begin{aligned} \mathrm{I^{F1}} &= \mathrm{I^{F1}_{MN}} + \mathrm{I^{F1}_{NM}}, \\ \mathrm{I^{F1}_{MN}} &= \mathrm{I_g} + \mathrm{I_{eq1}}, \\ \mathrm{I^{F1}_{NM}} &= \mathrm{I_{eq2}}, \end{aligned} \tag{3}$$

where I_g, I_{eq1} and I_{eq2} are the current contributions from the grid, equivalent converter interfaced DGs at bus M and N, respectively. The utility grid provides reactive power during fault. In addition, converter interfaced DGs also provide reactive component of current during fault [1]. This implies the currents contributed to the fault from both sides of the faulted line segment contains reactive component which lead to low power factor or large phase angle. The aforementioned is true for both grid-connected and islanded modes of converter dominated microgrid operations.

4.2 | Angle estimation using DFT

The proposed phase-angle-change-based protection scheme is equivalent to the principle of phase comparison method [37]. Unlike the phase comparison method, the proposed method does not compare the measured data of both ends of the line segment at the same instant, rather it uses the status of transition pattern (0 or 1) of the other end. The sinusoidal current signal of frequency f can be described by its magnitude and angular position with respect to an arbitrary time reference.

$$i(t) = I_m \cos(2\pi ft + \phi). \tag{4}$$

The phasor representation of $i(t)$ is given by

$$I = \frac{I_m}{\sqrt{2}} e^{j\phi}. \tag{5}$$

Using DFT,

$$I(k) = \frac{\sqrt{2}}{N} \sum_{n=0}^{N-1} i_{k+n} e^{\frac{-j2\pi n}{N}}, \tag{6}$$

where k is the first sample in data window and N is the number of samples in one-cycle of the fundamental frequency component. The real and imaginary parts are

$$I_{\mathrm{real}} = \frac{\sqrt{2}}{N} \sum_{n=0}^{N-1} i_n \cos\left(\frac{2\pi n}{N}\right), \tag{7}$$

$$I_{\mathrm{imag}} = \frac{\sqrt{2}}{N} \sum_{n=0}^{N-1} i_n \sin\left(\frac{2\pi n}{N}\right). \tag{8}$$

The magnitude of the phasor is the rms value of the sinusoid and the estimated angle of the phasor, $\phi = \tan^{-1}\left(\frac{-I_{imag}}{I_{real}}\right)$. The phase angle of current is continuously estimated using a window of one-cycle DFT for each sample, for example, n^{th} and $n^{th} + 1$ windows correspond to the phase angle of ϕ_n and ϕ_{n+1}, respectively. The change in phase angle is calculated as:

$$\Delta\phi(k) = \phi_n - \phi^{pre}, \tag{9}$$

where ϕ^{pre} is the phase angle of positive-sequence current phasor just before the fault detection and $\Delta\phi(k)$ ($k = 1,2,3\ldots$) is the change in phase angles in a window of DFT. Under normal condition, $\Delta\phi \approx 0$, for an internal fault, the change in angle $\Delta\phi$ will be negative at one end and positive at the other end of the line segment as discussed in Section 3.

TABLE 2 Protection decision for high resistance fault

I_{MN}			I_{NM}			
$\Delta\phi_{MN}$	ΔI_{MN1}	XOR	$\Delta Œ_{NM}$	ΔI_{NM1}	XOR	XOR
≤ 0 (0)	> 0 (1)	1	> 0 (1)	> 0 (1)	0	1
≤ 0 (0)	> 0 (1)	1	≤ 0 (0)	≤ 0 (0)	0	1

4.3 | Protection decision

The protection decision is taken based on the XOR operation of the signal generated at both ends of the line segment. As per the convention considered in this paper (refer Figure 5), during normal operating condition at any instant, the phase angle of current at one end of a line segment is $\phi°$ that of other end is $180 + \phi°$. For an internal fault, the phase angle of positive-sequence current changes in negative direction (corresponding signal 0) at 0° terminal and positive direction (corresponding signal 1) in 180° terminal. Figure 13 shows the phase angle comparison for trip decision during an internal fault. The unequal status of the generated signal at both ends results in a trip signal to the corresponding circuit breaker.

High resistance fault causes misoperation of relays as the direction of current does not alter during full load conditions at times, for example, in Case-3. Such a fault cannot be detected by only using the phase angle change information. Therefore, an additional feature is taken into account for protection decision correctly (Table 2). The sign of superimposed positive-sequence currents ΔI_{MN1} and ΔI_{NM1} are reported in addition with phase angle change information. In Section 3, Case 3 reveals the effect of high resistance fault in protection decision. In this case the change in phase angles in both cases are negative. However, $\Delta I_{NM1} = I_{NM1}^{Fi} - I_{NM1}^{pre} \leq 0$. In Figure 12, the flow chart of the proposed protection method is shown. Three phase currents are measured and one-cycle DFT is used to estimate the phasors. Then the positive-sequence current is obtained by using symmetrical components. Subsequently, the change in phase angle is calculated for protection decision.

For different types of loading as discussed in Section 3, the high resistance cannot be detected straight forward. The trip decision generation for all possible loading conditions are summarized in Figure 14. The exponential constants (n_p, n_q) for constant impedance, constant power, constant current loads are set as (1, 0), (0, 0) and (1, 1), respectively.

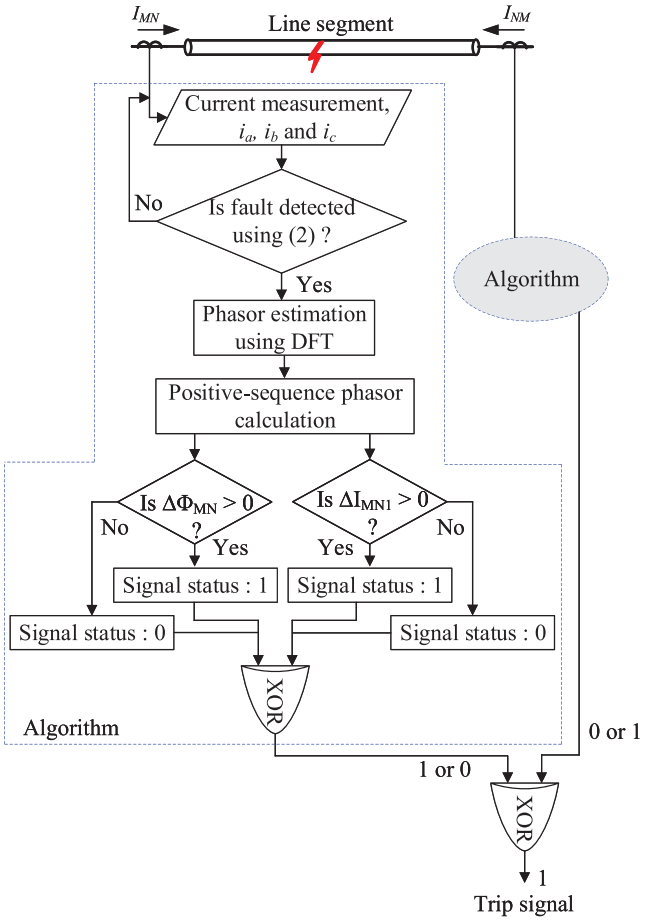

FIGURE 12 Flow chart of proposed protection method

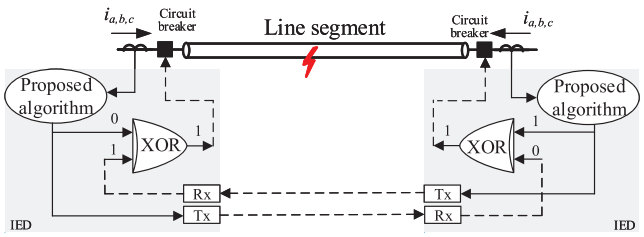

FIGURE 13 Phase angle comparison for trip decision

4.4 | Identification of status of communication channel

A logic is shown in Figure 15 to identify the operational status of communication channel. For the communication channel in operation, the output of the OR gate will always be 1 irrespective of the remote end pickup signal and the output of NOT gate (right hand side) is 0. In case of failure of communication channel, the output of OR gate becomes 0 (as both inputs to the OR gate are 0), and the NOT gate output will be 1. Therefore, the status of communication channel can be identified using the logic (Figure 15).

5 | RESULTS

A converter dominated medium-voltage microgrid with Petersen coil grounding as shown in Figure 1 is simulated using MATLAB Simulink. The simulation parameters are listed in Table 3. The three-phase currents are measured and sampled at a rate of 4 kHz. In the one-cycle DFT, 80 samples are used as the fundamental frequency of the system is 50 Hz. The positive-sequence component of current (I_1) is calculated using the three

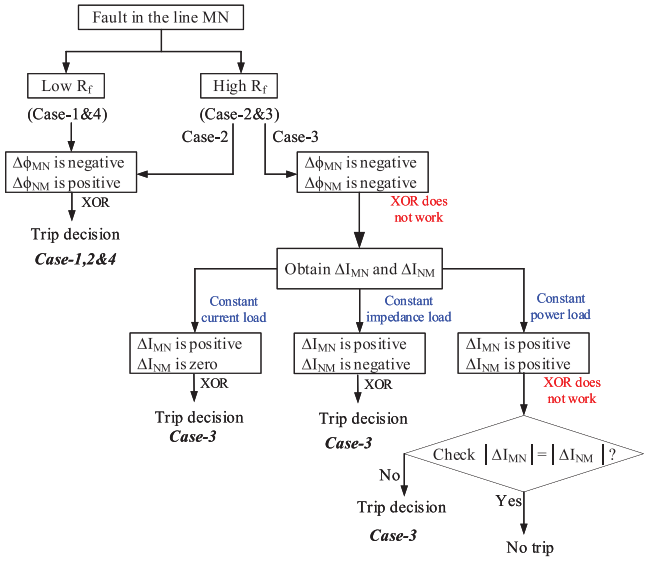

FIGURE 14 Trip decision generations for different types of loading

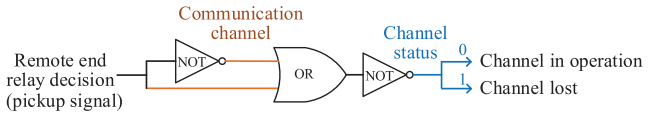

FIGURE 15 Identification of communication channel loss [38]

TABLE 3 System parameters

System voltage	10 kV
Base power	10 MVA
Frequency	50 Hz
Battery storage	2 MW, 1.2kAh, Lithium ion
Wind turbine	2 MW
Fault resistance	0 - 20 Ω
Fault location	1 - 99% of line length
Fault types	LG, LL, LLG, LLL
Loading:	
Constant impedance load	8 MW, n_p=1,n_q=0
Constant power load (V_{rated})	6 MW, 2.4 MVAr, n_p=n_q=0
Constant current load (V_{rated})	6 MW, 2.4 MVAr, n_p=n_q=1
Controller parameters:	
Controller bandwidth α_{cc}	500 Hz
K_p and K_i	39.47 and 118.43
Filter parameters:	
R_f and L_f	6 mΩ and 2 mH
Cable parameters:	
Cross-section area	240 mm^2
Resistance	0.125 Ω/km
Inductance	0.28 mH/km
Capacitance	0.48 μF/km

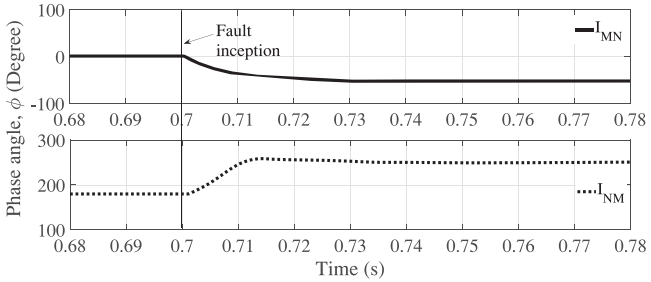

FIGURE 16 Phase angle of current at M and N for the internal fault

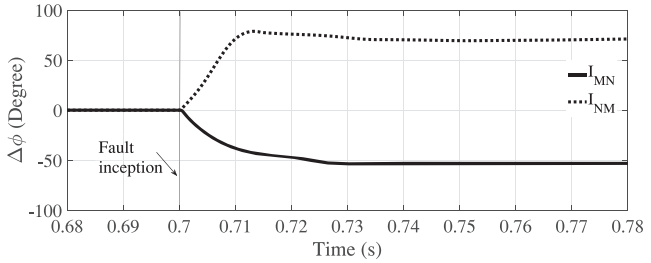

FIGURE 17 Phase angle change of current at M and N for the internal fault

phasors (I_a, I_b and I_c). The angle change of I_1 at both ends indicates the internal and external fault for the line segment to be protected. The performance of the proposed algorithm is tested for various cases including high resistance fault, bidirectional power flow, different types of fault and loading conditions. The simulation is carried out and results are shown for the power flow direction from M to N (refer Figure 1).

In this paper, the results for extensive test cases are shown for the power flow direction from M to N. However, for the opposite power flow direction, that is, from N to M, the proposed algorithm works well with only change in the swapping of generated status 0 to 1 and 1 to 0 at both ends. This has no effect on XOR operation as its output is 1 for unequal input status.

5.1 | Internal fault

A balanced three phase fault (F_1) is applied at the middle of the line segment MN shown in Figure 1. The fault is incepted at 0.7 s of simulation run with the fault resistance of 0.1 Ω. It is to be noted that the prefault power flow is from M to N. Figure 16 shows that the prefault phase angle of I_{MN} and I_{NM} are 0° and 180°, respectively. During F_1, the angle of I_{MN} ramps down to −54° and that of I_{NM} to 260°. The change in phase angle of I_{MN} and I_{NM} is negative and positive, respectively, which is evident from Figure 17. As a result, the protection decision is taken at relay M_2 based on XOR operation of the generated signal 1 and received signal 0. Similarly, at N_1 the generated and received signals are 0 and 1, respectively. XOR of 0 and 1 at N_1 results in 1 and hence the trip signal is generated.

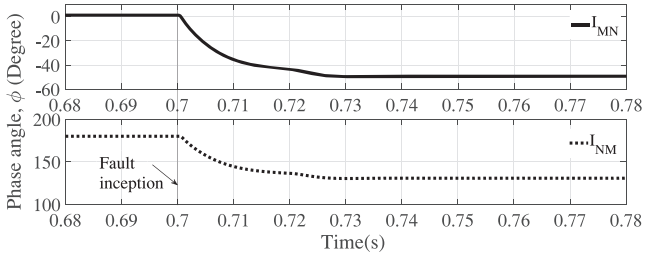

FIGURE 18 Phase angle of current at M and N for the external fault

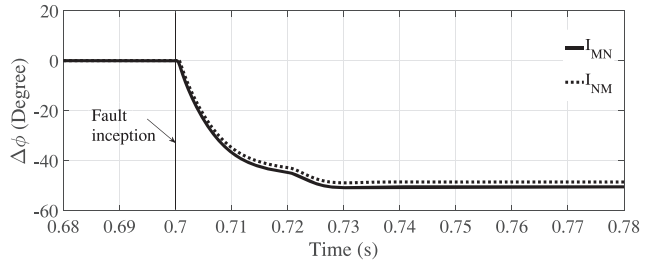

FIGURE 19 Phase angle change of current at M and N for the external fault in the same direction of power flow

5.2 | External fault in the direction of power flow

The fault (F_2) in the line segment NJ in Figure 1 is considered as an external fault for the line segment MN. F_2 is a three phase fault with a resistance of 0.5 Ω created at 0.7 s at the middle of the line segment NJ. Before the fault F_2, the power flow was from bus M to bus N. The phase angle of I_{MN} and I_{NM} are shown in Figure 18. The change in phase angles are negative in both ends of the line segment MN and are plotted in Figure 19. Therefore, no trip signal will be generated as relay at both ends transmit and receives the signal status 0 which is correct.

5.3 | External fault with the reverse power flow

The performance of the proposed algorithm is also tested for the reverse power flow case. In this case, power flow was from N to M before the external fault (F_2) which is evident from the phase angle of I_{MN} and I_{NM} as shown in Figure 20. The change in phase angles are positive for both I_{MN} and I_{NM} as depicted in Figure 21. So, no trip signal will be derived.

5.4 | Fault on a radial line during no load

The performance of the algorithm is tested for no load condition of a radial, single source unidirectional power flow line segment. Prefault power flow in the line MN is considered to be zero before the fault. A three phase fault is created at the middle of the line MN in Figure 1 and the change in phase angle ($\Delta\phi$) of I_{MN} and I_{NM} is observed. It is found that $\Delta\phi$ of I_{MN} is negative and that of I_{NM} is zero as shown in Figure 22. Being no source present at N, there is no current I_{NM} even during fault. The protection decision in such case is taken using the change in phase angle and superimposed positive-sequence component of I_{MN}.

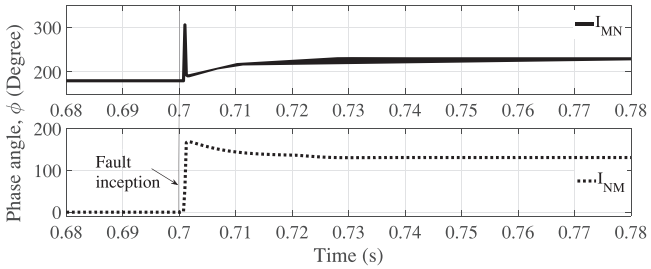

FIGURE 20 Phase angle of current at M and N for the external fault opposite to power flow

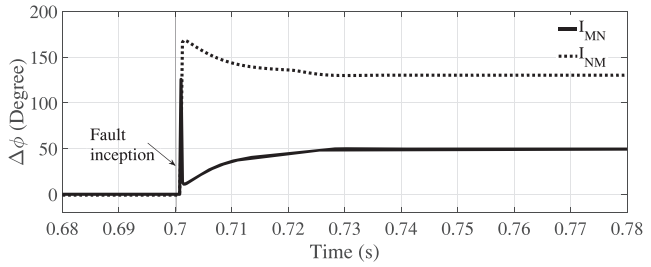

FIGURE 21 Phase angle change of current at M and N for the external fault in the opposite direction of power flow

5.5 | High resistance fault

A high resistance line-to-ground fault with 20 Ω is created at the middle of the line segment MN at 0.7 s of the simulation run. The change in phase angle of currents at M and N are found to be negative which is evident from Figure 23. The corresponding generated signals due to the negative change of phase angles are 0 at both ends. The superimposed positive-sequence current magnitude ΔI_{MN1} and that of ΔI_{NM1} are positive (signal status 1) and negative (signal status 0), respectively. Finally, the XOR operation of the generated and received signals produces the trip command.

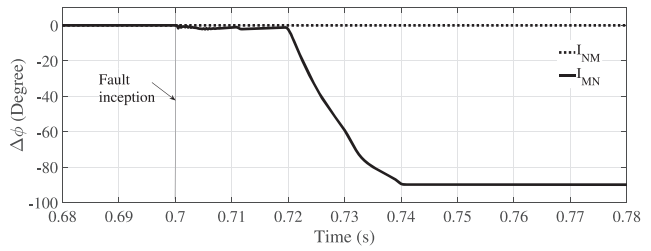

FIGURE 22 Phase angle change of current at M and N for an internal fault during no load condition

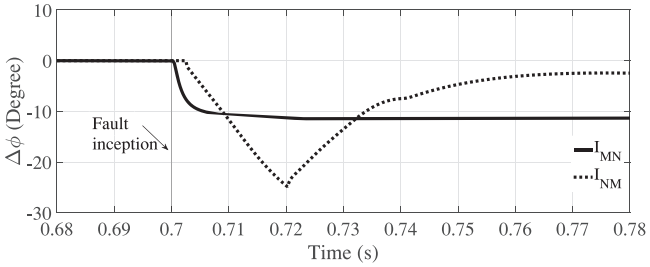

FIGURE 23 Phase angle change of current at M and N for a high resistance internal fault

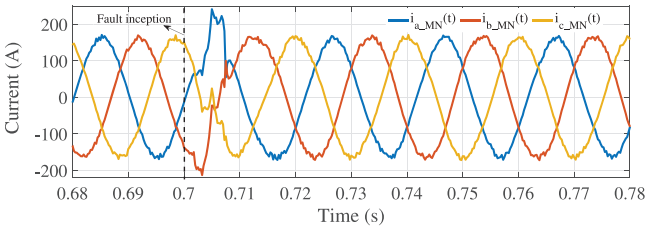

FIGURE 24 Three phase current signals at M for the LG fault with noise

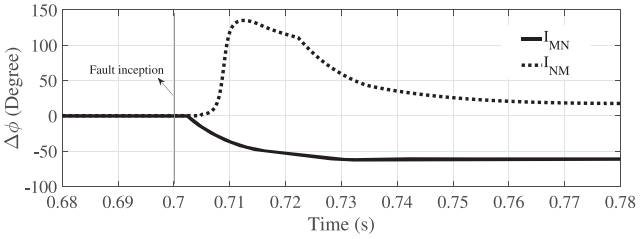

FIGURE 25 Phase angle change of current at M and N for the LG fault in noisy environment

5.6 | Fault during different power factor loading

The performance of the proposed algorithm is verified for loading conditions with different power factors. Such case studies are important because, the phase angle of prefault current depends upon the load power factor. Loading of 0.8 lagging, unity and 0.8 leading power factors at bus N are considered separately and different faults are created in the line segment MN. The change in phase angles of I_{MN} and I_{NM} are summarized in Table 4. The phase angle change with opposite sign at both ends of the line segment generates the trip signal using XOR operation.

5.7 | Performance with noisy signals

The performance of the proposed method is tested for current signals contaminated with uniform distribution noise with zero mean and a standard deviation of 3% [39]. A LG fault (phase-a-to-ground) is simulated at 0.7 s at F_1 in the line segment MN (Figure 1). The noisy current signal during the fault is shown in Figure 24. Using the proposed current's phase-angle-change-based protection technique, the $\Delta\phi$ is computed as shown in Figure 25. It is observed that the change in phase angle of I_{MN} and I_{NM} are negative and positive, respectively, which confirms F_1 as an internal fault even with noisy environment. The proposed method uses one-cycle DFT for phasor estimation to obtain the corresponding phase angle of current which has the inherent filtering capability that takes care the noise in the signals.

5.8 | Performance for different fault location

The performance of the method is validated for different fault location in the line segment MN (Figure 1). In this case, three-phase fault is applied at distance of 2%, 30%, 50%, 80% and 98% of the line length MN from bus M. For all cases, the $\Delta\phi$ is obtained as shown in Figure 26 where it is clearly evident that the proposed method is correctly identifying the faults in the line segment MN irrespective of fault locations.

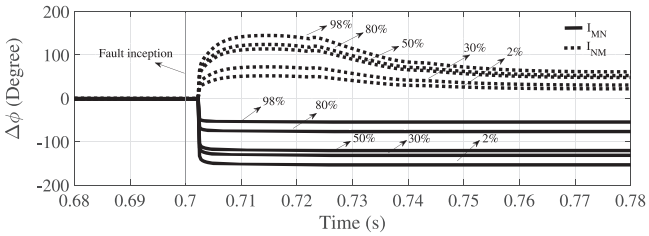

FIGURE 26 Phase angle change of both end currents for different fault locations in the line segment MN

TABLE 4 Change in phase angle of current at M and N during different loading conditions

Fault types	Load power factor at bus N								
	0.8 lagging			unity			0.8 leading		
	$\Delta\phi_{MN}$	$\Delta\phi_{NM}$	XOR	$\Delta\phi_{MN}$	$\Delta\phi_{NM}$	XOR	$\Delta\phi_{MN}$	$\Delta\phi_{NM}$	XOR
Line-to-ground fault (LG)	−41°	80°	1	−74°	76°	1	−41°	35°	1
Double line-to-ground fault (LLG)	−38°	62°	1	−73°	57°	1	−35°	41°	1
Line-to-line fault (LL)	−44°	48°	1	−76°	60°	1	−44°	52°	1
Three phase to ground fault (LLLG)	−48°	95°	1	−72°	88°	1	−46°	44°	1
Three phase fault (LLL)	−46°	84°	1	−78°	85°	1	−82°	32°	1

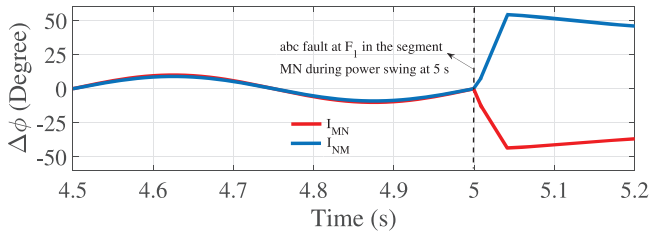

FIGURE 27 $\Delta\phi$ of both end currents for F_1 in the line segment MN during power swing

5.9 | Performance during power swing

There may be a chance of power swing following the fault in islanded microgrid with multiple synchronous-based DGs [40]. The phase angle of current (ϕ) changes with the variation of voltage angle (δ) during power swing as shown below [41]

$$\Delta\phi \propto \Delta\delta. \tag{10}$$

If $\Delta\delta$ is positive, $\Delta\phi$ will be positive and vice-versa. To test the performance of the proposed protection method, a power swing case is simulated for the system shown in Figure 1 by replacing all the converter interface DGs with synchronous-based DG. The voltage and current signals get modulated with low frequency component (in this case 2 Hz). A three-phase fault (F_1) is created at the middle of the line MN at 5 s during power swing. The phase angle change of current ($\Delta\phi$) at both ends of the line segment MN is obtained using the proposed method for swing conditions with and without fault. It is seen that $\Delta\phi$ is oscillating between positive and negative values of small magnitude during power swing even with no fault (before t = 5 s in Figure 27). However, both ends $\Delta\phi$ changes simultaneously in positive (both ends binary output 1) and negative (both ends binary output 0) directions resulting in the XOR output of 0. Therefore, no trip signal will be generated for the circuit breaker. The proposed method sees the power swing as an external phenomenon, which is correct. However, for the fault during power swing at 5 s, both ends $\Delta\phi$ changes in opposite directions resulting in a trip signal. Thus, the proposed method accurately distinguishes power swing and fault conditions.

The scalability and repeatability are the preliminary requisites of any proposition to perform scaling-up and repetition successfully. The technical aspect of scalability and repeatability of the proposed protection method is studied through different test cases. The proposed protection algorithm determines the direction of fault using the phase angle change of local current data. The protection decision is derived in case of IEDs at both ends of the line to see the fault in forward direction. Both end's phase angle change information being used, the proposed method is suitable for bidirectional flow case, and thus, its applicability can be scaled-up to both radial and meshed network protection. Since magnitude of current is not required for protection decision, the usefulness of the proposed method is successfully tested for microgrid with converter interfaced sources that limits the fault current within 1 per unit. Other technical factors such as different fault resistance, fault location, fault types and noise in the signals are also considered and the performance of the proposed method is found satisfactory. From economic aspect perspective, the proposed method uses only local current data for the protection decision. A low bandwidth communication channel is required for the exchange of binary information only during fault. Since voltage data is not used in the proposed method, additional cost due to the installation of voltage transformer is saved.

6 | DISCUSSION

This work presents the analysis and investigation of current's phase angle change for converter with and without reactive power support during fault condition. The behavior of grid forming and grid feeding converters during a fault to stay synchronized to the grid and provide best support to the grid is a very relevant and interesting topic. The effect of different control strategies on proposed protection setting is also worth further investigation.

The current phasor is estimated using one-cycle DFT for a sampling frequency of 4 kHz. Along with prefault, another half-cycle (10 ms for a 50 Hz system) data window during fault is required for accurate phasor estimation followed by the correct protection decision. The latency of available communication link (much lesser than 10 ms) is therefore not an issue for the proposed phasor-based protection method [42].

7 | CONCLUSION

In this paper, phase angle change of current-based protection algorithm with detailed theoretical analysis is proposed for converter dominated microgrids. The proposed algorithm uses the change in phase angle of positive-sequence current at both ends of the line segment to derive the protection decision. High resistance fault is detected using change in magnitude of current, even if the direction of power flow does not overturn at the other end of the faulted segment. Furthermore, the proposed algorithm does not need remote end data continuously, which require a low bandwidth communication channel. The implementation of the algorithm is easy, simple and economic as it uses only current data and can be a modified feature of available current-based intelligent electronic devices. Also, the proposed protection method is a reliable solution for microgrids with and without mesh configuration as it uses both ends current measurement and transfers the trip decision to remote end. The future work is to develop a centralized protection of microgrids robust to communication delay and link failures.

ACKNOWLEDGEMENT

This work is supported by Energy Area of Advance at Chalmers University of Technology, Sweden under the Project No. WP A6, Sweden Energy Agency under SamspEL program with project number P43014-1 and FLEXI-GRID, European

Community's Horizon 2020 Framework Programme under grant agreement no.: 864048.

CONFLICT OF INTEREST

The authors declare no conflict of interest.

NOMENCLATURE

A. Abbreviation

BESS	Battery energy storage system
DFT	Discrete Fourier Transform
DG	Distributed generation
FDF	Forward direction fault
MV	Medium-voltage
PC	Petersen coil
PV	Photovoltaic
RDF	Reverse direction fault
VSC	Voltage source converter
XOR	Exclusive OR logic gate

B. Subscripts

(a, b, c)	Phase-a, Phase-b, Phase-c
(d, q, n)	d-, q-axis components, n^{th} sample
(real, imag)	Real and imaginary parts
(1, 2, 0)	Positive-, negative-, zero-sequence components

C. Superscripts

*	Reference
(F_1, F_2)	Signals during fault
(*pre*)	Prefault signals

D. Variables

I_d	Active component of current
I_q	Reactive component of current
I_{MN}	Current at M bus in the line segment MN
I_{NM}	Current at N bus in the line segment MN
P	Active power flow
Q	Reactive power flow
V_d	d-axis component of voltage
V_n	Neutral voltage
V_q	q-axis component of voltage
V_1	Positive-sequence voltage
Z_{eq1}	Equivalent impedance of DG-1
Z_{eq2}	Equivalent impedance of DG-2
Z_g	Equivalent impedance of the grid
ϕ	Phase angle of current
$\Delta\phi$	Change in current's phase angle

ORCID

Rabindra Mohanty https://orcid.org/0000-0003-3514-850X

REFERENCES

1. Hooshyar, A., Iravani, R.: Microgrid protection. Proc. IEEE 105(7), 1332–1353 (2017)
2. Perveen, R., Kishor, N., Mohanty, S.R.: Fault detection for offshore wind farm connected to onshore grid via voltage source converter-high voltage direct current. IET Gener., Transm. Distrib. 9(16), 2544–2554 (2015)
3. Singh, P., Pradhan, A.K.: A local measurement based protection technique for distribution system with photovoltaic plants. IET Renew. Power Gener. 14(6), 996–1003 (2020)
4. Xin, Z., Wang, L., Jiang, H., Chai, B., Yang, J.: Smart re-close scheme of combined overhead line with underground power cable. In: 2010 International Conference on Power System Technology, pp. 1–6. IEEE, Piscataway (2010)
5. Wang, P., Zhou, H., Baichao, C., Tian, C., Chen, B., Sun, B.: A novel ground-fault location method in resonant grounded networks based on distributed modulation and compensation adjustment. IEEE Trans. Power Deliv. 34(5), 1938–1947 (2018)
6. Wang, P., Chen, B., Zhou, H., Cuihua, T., Sun, B.: Fault location in resonant grounded network by adaptive control of neutral-to-earth complex impedance. IEEE Trans. Power Deliv. 33(2), 689–698 (2018)
7. Zarei, S.F., Mokhtari, H., Blaabjerg, F.: Fault detection and protection strategy for islanded inverter-based microgrids. IEEE J. Emerging Selected Topics Power Electron. 9(1), 472–484 (2019)
8. Gadde, P.H., Brahma, S.: Realistic microgrid test bed for protection and resiliency studies. In: 2019 North American Power Symposium (NAPS), pp. 1–6. IEEE, Piscataway (2019)
9. Microgrid Protection systems.: Working Group C30, Subcommittee C of the Power System Relaying and Control Committee (2019)
10. Gururani, A., Mohanty, S.R., Mohanta, J.C.: Microgrid protection usinf Hilbert-Huang transform based-differential scheme. IET Gener., Transm. Distrib. 10(15), 3707–3716 (2016)
11. Sortomme, E., Ren, J., Venkata, S.S.: A differential zone protection scheme for microgrids. In: 2013 IEEE Power Energy Society General Meeting, pp. 1–5. IEEE, Piscataway (2013)
12. Brahma, S.: Protection of distribution system islands fed by inverter-interfaced sources. In: 2019 IEEE Milan PowerTech, pp. 1–6. IEEE, Piscataway (2019)
13. Mishra, P., Pradhan, A.K., Bajpai, P.: Voltage control of pv inverter connected to unbalanced distribution system. IET Renew. Power Gener. 13(9), 1587–1594 (2019)
14. Nsengiyaremye, J., Pal, B.C., Begovic, M.M.: Microgrid protection using low-cost communication systems. IEEE Trans. Power Delivery 35(4), 2011–2020 (2019)
15. Li, X., Dyśko, A., Burt, G.M.: Traveling wave-based protection scheme for inverter-dominated microgrid using mathematical morphology. IEEE Trans. Smart Grid 5(5), 2211–2218 (2014)
16. Mishra, P., Pradhan, A.K., Bajpai, P.: A positive sequence relaying method for solar photovoltaic integrated distribution system. IEEE Trans. Power Deliv. early access (2020)
17. Ataei, M.A., Gitizadeh, M., Lehtonen, M., Razavi Far, R.: Multi-agent based protection scheme using current-only directional overcurrent relays for looped/meshed distribution systems. IET Gener., Transm. Distrib. 1–15 (2021)
18. Al-Nasseri, H., Redfern, M.A., O'Gorman, R.: Protecting micro-grid systems containing solid-state converter generation. In: 2005 International Conference on Future Power Systems, pp. 1–5. IEEE, Piscataway (2005)
19. Sati, T., Azzouz, M.A.: Optimal protection coordination for inverter dominated islanded microgrids considering N-1 contingency. IEEE Trans. Power Delivery 1–1 (2021)
20. Wang, B., Jing, L.: A protection method for inverter-based microgrid using current-only polarity comparison. J. Modern Power Syst. Clean Energy 8(3), 446–453 (2020)
21. Parhizi, S., Lotfi, H., Khodaei, A., Bahramirad, S.: State of the art in research on microgrids: A review. IEEE Access 3, 890–925 (2015)
22. Bakkar, M., Bogarra, S., Córcoles, F., Iglesias, J.: Overcurrent protection based on ANNs for smart distribution networks with grid-connected VSIs. IET Gener., Transm. Distrib. 15(7), 1159–1174 (2021)
23. de la Barra, J., Angulo, A., Gil, E.: A model for simultaneous location and coordination of protective devices in radial distribution networks. IET Gener., Transm. Distrib. 15(19), 2734–2746 (2021)
24. Singh, M.: A q component-based adaptive protection coordination optimisation using overcurrent relays in coordination with fuses for hybrid microgrid. IET Gener., Transm. Distrib. 15(14), 2061–2074 (2021)

25. Barik, M.A., Gargoom, A., Mahmud, M.A., Haque, M.E., Al-Khalidi, H., Than Oo, A.M.: A decentralized fault detection technique for detecting single phase to ground faults in power distribution systems with resonant grounding. IEEE Trans. Power Deliv. 33(5), 2462–2473 (2018)
26. Li, Y., Jiao, S., Zhang, C.: Safety analysis on pilot zero sequence direction relay application in parallel lines. Autom. Electr. Power Syst. 32, 104–107 (2008)
27. Mooney, J., Peer, J.: Application guidelines for ground fault protection. Paper presented at the 1998 international conference on modern trends in the protection schemes of electric power apparatus and systems, New Delhi, India, 28–30 October 1998
28. Mohanty, R., Chen, P., Tuan, L.A., Narula, A.: Challenges in protection of converter dominated medium-voltage microgrids. In: 2019 IEEE PES Innovative Smart Grid Technologies Europe (ISGT-Europe), pp. 1–5. IEEE, Piscataway(2019)
29. Bollen, M., Styvaktakis, E.: Tutorial on voltage sag analysis. In: Ninth International Conference on Harmonics and Quality of Power, vol. 1, pp. 193–194. IEEE, Piscataway (2000)
30. Kim, S.D., Morcos, M.M., Gomez, J.C.: Voltage-sag magnitude and phase jump due to short circuits in distribution systems with variable fault resistance. Electr Power Compon Syst. 33(5), 493–512 (2006)
31. Jia, J., Yang, G., Nielsen, A.H.: A review on grid-connected converter control for short-circuit power provision under grid unbalanced faults. IEEE Trans. Power Deliv. 33(2), 649–661 (2018)
32. Zhang, F., Mu, L.: A fault detection method of microgrids with grid-connected inverter interfaced distributed generators based on the PQ control strategy. IEEE Trans. Smart Grid 10(5), 4816–4826 (2019)
33. Grid code.: In: High and Extra High Voltage. E.ON Netz BmbH, Bayreuth (2006)
34. Valentini, M., Akhmatov, V., Iov, F., Thisted, J.: Fault current contribution from VSC-based wind turbines to the grid. In: The Second International Symposium on Electrical and Electronics Engineering, (ISEEE), pp. 1–7. IEEE, Piscataway (2008)
35. Application provision.: In: Regional Network Tariffs, pp. 1–39. Vattenfall Eldistribution AB, Sweden, (2016)
36. Jalilian, A., Hagh, M.T., Hashemi, S.M.: An innovative directional relaying scheme based on postfault current. IEEE Trans. Power Delivery 29(6), 2640–2647 (2014)
37. Eissa, M.M.: A novel centralized wide area protection "CWAP" in phase portrait based on pilot wire including phase comparison. IEEE Trans. Smart Grid 10(3), 2671–2682 (2019)
38. Jahromi, A.A., Kemmeugne, A., Kundur, D., Haddadi, A.: Cyber-physical attacks targeting communication-assisted protection schemes. IEEE Trans. Power Syst. 35(1), 440–450 (2020)
39. Mohanty, R., Pradhan, A.K.: Protection of smart dc microgrid with ring configuration using parameter estimation approach. IEEE Trans. Smart Grid 9(6), 6328–6337 (2018)
40. Fayazi, H., Moazzami, M., Fani, B., Shahgholian, G.: A first swing stability improvement approach in microgrids with synchronous distributed generators. Int. Trans. Electr. Energy Syst. 31(4), e12816 (2021)
41. Khodaparast, J., Khederzadeh, M., da Silva, F.F., Leth Bak, C.: Power swing detection in upfc-compensated line by phase angle of current. IEEE J. Emerging Selected Topics Circuits Syst. 7(3), 459–468 (2017)
42. Liu, S., Liu, D.: A high-flexible low-latency memory-based fft processor for 4G, wlan, and future 5G. IEEE Trans. Very Large Scale Integr. (VLSI) Syst. 27(3), 511–523 (2019)

How to cite this article: Mohanty, R., Chen, P., Tuan, L.A.: Protection of converter dominated MV microgrid using changes in current's phase angle. IET Gener. Transm. Distrib. 1–13 (2021).
https://doi.org/10.1049/gtd2.12317